Research Square

Preprints are preliminary reports that have not undergone peer review.
They should not be considered conclusive, used to inform clinical practice,
or referenced by the media as validated information.

Comparison of Structural and Mechanical Properties of Heat-treated Ti-6al-4v Alloy Obtained by Additive Manufacturing and Metallurgical Routes

Andrii Burmak

burmak@kpm.kpi.ua

National Technical University of Ukraine Igor Sikorsky Kyiv Polytechnic Institute: Nacional'nij tehnicnij universitet Ukraini Kiivs'kij politehnicnij institut imeni Igora Sikors'kogo https://orcid.org/0000-0003-2415-8032

Mykhailo Voron

National Technical University of Ukraine Igor Sikorsky Kyiv Polytechnic Institute: Nacional'nij tehnicnij universitet Ukraini Kiivs'kij politehnicnij institut imeni Igora Sikors'kogo

Serhiy Schwab

Institut elektrozvaruvanna imeni E O Patona Nacional'na akademia nauk Ukraini

Ievgen Byba

National Technical University of Ukraine Igor Sikorsky Kyiv Polytechnic Institute: Nacional'nij tehnicnij universitet Ukraini Kiivs'kij politehnicnij institut imeni Igora Sikors'kogo

Igor Vladymyrskyi

National Technical University of Ukraine Igor Sikorsky Kyiv Polytechnic Institute: Nacional'nij tehnicnij universitet Ukraini Kiivs'kij politehnicnij institut imeni Igora Sikors'kogo

Svitlana Voloshko

National Technical University of Ukraine Igor Sikorsky Kyiv Polytechnic Institute: Nacional'nij tehnicnij universitet Ukraini Kiivs'kij politehnicnij institut imeni Igora Sikors'kogo

Research Article

Keywords: additive manufacturing, Ti-6Al-4V, SLM, WAAM, heat treatment, structural-phase state

Posted Date: March 2nd, 2026

DOI: https://doi.org/10.21203/rs.3.rs-8831437/v1

License: This work is licensed under a Creative Commons Attribution 4.0 International License.
Read Full License

COMPARISON OF STRUCTURAL AND MECHANICAL PROPERTIES OF HEAT-TREATED Ti-6Al-4V ALLOY OBTAINED BY ADDITIVE MANUFACTURING AND METALLURGICAL ROUTES

Andrii Burmak[1*], ORCID 0000-0003-2415-8032
Mykhailo Voron[1,2], ORCID 0000-0002-0804-9496
Serhiy Schwab[3], ORCID 0000-0002-4627-9786
Ievgen Byba[1,4], ORCID 0000-0002-1696-300X
Igor Vladymyrskyi[1], ORCID 0000-0002-2106-9176
Svitlana Voloshko[1], ORCID 0000-0003-3170-8362

[1]*National Technical University of Ukraine "Igor Sikorsky Kyiv Polytechnic Institute", 37, Beresteiskyi Ave, Kyiv, 03056, Ukraine*
[2]*Physico-Technological Institute of Metals and Alloys of the National Academy of Sciences of Ukraine, 34/1, Vernadsky Blvd., Kyiv, 03142, Ukraine*
[3]*E.O. Paton Electric Welding Institute of the National Academy of Sciences of Ukraine, 11, Kazymyr Malevich St., Kyiv, 03150, Ukraine*
[4]*Institute of Applied Control Systems of the National Academy of Sciences of Ukraine, 40, Akademika Glushkova Ave, Kyiv, 03187, Ukraine*
*Corresponding author, e-mail: burmak@kpm.kpi.ua

Abstract

This study is devoted to the structural and mechanical properties of Ti-6Al-4V alloy in the as-received state obtained by various 3D printing approaches – selective laser melting (SLM) and wire arc additive manufacturing (WAAM), as well as to evolution of the properties under different heat treatment parameters. The obtained results were compared with a conventionally produced industrial counterpart – an electrometallurgical ingot, hot-rolled into a rod. The results suggest significant differences in microstructure (e.g., grain size, phases distribution and morphology), phase composition, and mechanical properties between additively manufactured materials and hot-rolled counterparts. Moreover, the applied heat treatment procedures directly influence the structural homogeneity, the degree of crystal lattice distortion, formation of the martensitic phase, and the dispersion of secondary phases, determining the microhardness of the investigated t materials.Thus, it is shown that mechanical properties of the Ti-6Al-4V alloy could be effectively controlled by selection of the appropriate manufacturing technology and heat treatment conditions.

Keywords: additive manufacturing, Ti-6Al-4V, SLM, WAAM, heat treatment, structural-phase state

1 Introduction

Additive manufacturing (AM) is a process based on the step-by-step addition of a material onto a substrate, as opposed to traditional mechanical processing, which involves the incremental removal of the material. 3D printing can surpass conventional metallurgical production in terms of massiveness, economic and technological efficiency,

since it eliminates the need for tooling, additional metal costs, and enables faster adaptation to changing market demands. Thus, AM becomes a new driving force of the ongoing industrial revolution. However, for its widespread industrial adoption, two critical challenges have to be overcome – lowering the cost of powders or wires as printing materials, and enhancing the mechanical properties of printed components to overcome characteristics of traditionally obtained counterparts [1-4].

The most commonly used method for metal products AM is a selective laser melting (SLM) of metal powder [3]. In this case, the laser power typically ranges from 100 to 1000 W, and the thickness of each melted powder layer lies in the range of 20 – 100 μm, providing an advantage compared to other AM processes in terms of the resolution. Efficiency of this method primarily depends on the dispersity and quality of the used powders [5].

Metallic materials, in particular Ti-based alloys, produced by the SLM exhibit higher levels of residual stresses, a more pronounced non-equilibrium phase state, increased strength, fatigue resistance, and reduced ductility compared to similar metallurgical products [3, 6, 7]. This is due to the differences in the heat impact from the energy source, type of consumable material, and the completeness of its melting, as well as the specifics of the subsequent heat dissipation, which directly affect crystallization, structural phase transitions within the volume of additively manufactured parts. In such case, heat treatment seems to be most valuable tool to control structure and properties of 3D-manufactured materials.

Heat treatment of additively manufactured products made of titanium alloys is a recommended procedure to enhance their structural and mechanical properties [8]. In particular, for components manufactured from the Ti–6Al–4V (Grade 5) alloy, with a metal powder used as expendable material, thermal post-annealing is commonly applied. Such treatment involves a heating to the required temperature, holding for 1 – 1.5 hours with the following cooling in the furnace. Incomplete low-temperature annealing within the 450 – 750°C range enables the elimination of martensite-like α’-phase, reducing the hardness and increasing the ductility of the products. Annealing in the two-phase α+β region at temperatures of 800 – 950°C for 4 – 8 hours allows to optimize the structure and enhance the materials ductility. Full annealing above 980 – 1000 °C is rarely used due to the rapid growth of β-grains, negatively affecting formation of the final structure and the mechanical properties [7].

Quenching and aging of Ti–6Al–4V components produced by the SLM method are rarely applied [8-10] due to the fact that the as-received microstructure typically consists of fine acicular α’ martensite and other non-equilibrium phases providing high strength and limiting the effectiveness of conventional heat-treatment routes. The yield strength and ultimate tensile strength of SLM-processed alloy slightly exceed those achieved by conventional metallurgical routes (950 MPa and 1000 MPa versus 877 MPa and 985 MPa), whereas the elongation of AM parts is lower due to the presence of residual porosity [11]. Other AM techniques that employ solid or metal-filled flux-cored wires as feedstock are characterized by relatively low geometric precision, however, demonstrate high manufacturing productivity and a low level of internal defects. These processes mainly include electron beam–based and argon arc–based technologies, such as electron beam welding (EBW) and wire arc additive manufacturing (WAAM).

EBW-produced samples of the Ti–6Al–4V alloy usually reveal structural and phase characteristics similar to those of the as-cast state. Thus, in this case it is almost pointless to apply low-temperature annealing to eliminate the α'-phase and relieve stresses. Instead, the removal of the columnar and Widmanstätten structures mainly relies on annealing in the two-phase (α+β) region or by quenching followed by aging [6, 12, 13].

The process closest to EBW in terms of productivity and the properties of the resulting metal products is the WAAM technology, which is simpler and more convenient, does not require a vacuum, and is much less restricted in terms of workspace. This technology also relies on the use of a concentrated heat source to melt the metal, and Ar flow can be used as the protective atmosphere.

WAAM, in comparison with powder-based methods, achieves ~100% material utilization, as well as significantly higher productivity, making it highly justified for large-scale products. The equipment cost for such production is also substantially lower compared to the technologies based on electron beam or laser sintering [14-16]. The feasibility of Ti parts manufacturing using the WAAM approach is proved in [17]. The authors note that this technology remains minimally implemented so far due to the lack of equipment manufacturers offering ready-made industrial solutions and the limited choice of consumable materials.

Comparison of the mechanical properties of the Ti-6Al-4V alloy, manufactured by various technologies such as SLM, selective laser sintering, and WAAM, shows that the most significant anisotropy level of structure and properties is typical for WAAM-obtained parts [18]. This fact indicates the need to optimize technological regimes for 3D components production and to apply various surfaces and heat treatment regimes. Nevertheless, the WAAM technology could become the most effective alternative to the traditional metallurgical production of elements based on Ti alloys for aviation applications [19, 20].

While SLM-structure of Ti-6Al-4V is rather predictable, WAAM method may provide various structure and properties settings [21]. For example, WAAM-printed Grade 5 microstructure exhibits layering and signs of dendritic formation, resulting from the repetitive thermal cycles that occur during the layer-by-layer welding process. Regarding the mechanical properties, the yield strength and ultimate tensile strength of such samples are lower compared to the metallurgically produced alloy, and the ductility and fatigue strength are higher compared to the deformed samples produced by traditional technologies [22-24].

Although the microstructure of WAAM-printed Ti alloys is relatively homogeneous within each deposited layer, the structural components sizes and the quantitative phase ratios can vary several times through different areas of the additively manufactured part [25, 26]. Epitaxial growth of the primary β-phase and structural heterogeneities could lead to the mechanical properties anisotropy. Subsequent heat treatment can lead to effective grain refinement, anisotropy elimination, and a high level of mechanical properties of WAAM-printed Grade 5.

The popularity of WAAM and SLM AM processes is constantly increasing [25–28]. However, determination of the heat treatment effect on the structural and phase homogenization of Ti alloys is still a relevant research issue.

This study aims to compare the structural properties and microhardness of the Ti–6Al–4V alloy, produced by SLM and WAAM AM methods, with the industrial deformed rod-like product, in the initial as-produced state and after various heat treatment regimes.

2 Experimental procedure

As an industrial metallurgical product, Ti–6Al–4V alloy was used in the form of a hot-rolled rod with a diameter of 20 mm. It reveals a homogeneous fine-grained structure, which is sensitive to a heat treatment. Therefore, this alloy sample was used as a reference for comparison with the microstructure of materials obtained by SLM and WAAM methods, both after production and after various heat treatment regimes.

Ti–6Al–4V alloy samples were SLM-manufactured in the form of a 20×10×5 mm^3 parallelepiped using the Alfa-150D printer from «ALT Ukraine». The laser nominal power with a wavelength of 1070 ± 2 nm was 200 W, the focal diameter of the laser beam was 45 μm, the scanning speed was 500 mm/s, the layer thickness was 25 μm, and the hatch spacing was 150 μm. Spherical powder of the Ti–6Al–4V alloy with a particle size in the range of 15 – 53 μm, manufactured by «ALT Ukraine», was used for the printing. To prevent oxidation, the samples were produced in an inert Ar environment.

The WAAM samples were fabricated by TIG (Tungsten Inert Gas) process [29]. As a filler material, 2 mm diameter Grade 5 wire was deposited on a plate made from the same alloy in an Ar environment. The process was conducted under the following conditions: welding current 160 – 180 A, arc voltage 10.5 V, welding speed 8 m/h, feed rate 35 m/h, arc length 3 mm. As a result, a 7-layer product with 160 mm length, 10.5 mm height, and 10 mm width was produced. The experimental samples were subsequently cut from this product.

The chemical composition of the experimental samples was determined by X-ray fluorescence spectroscopy method (Table 1) and their appearance is illustrated in Fig. 1.

Table 1 Chemical composition of Ti-6Al-4V alloy samples produced by different methods

Production method	Chemical composition, mas. % (Ti – base)			
	Al	V	Si	Fe
Hot-rolled	5.81	4.17	0.043	0.15
SLM	5.71	4.17	0.045	0.15
WAAM	6.54	4.55	0.052	0.13

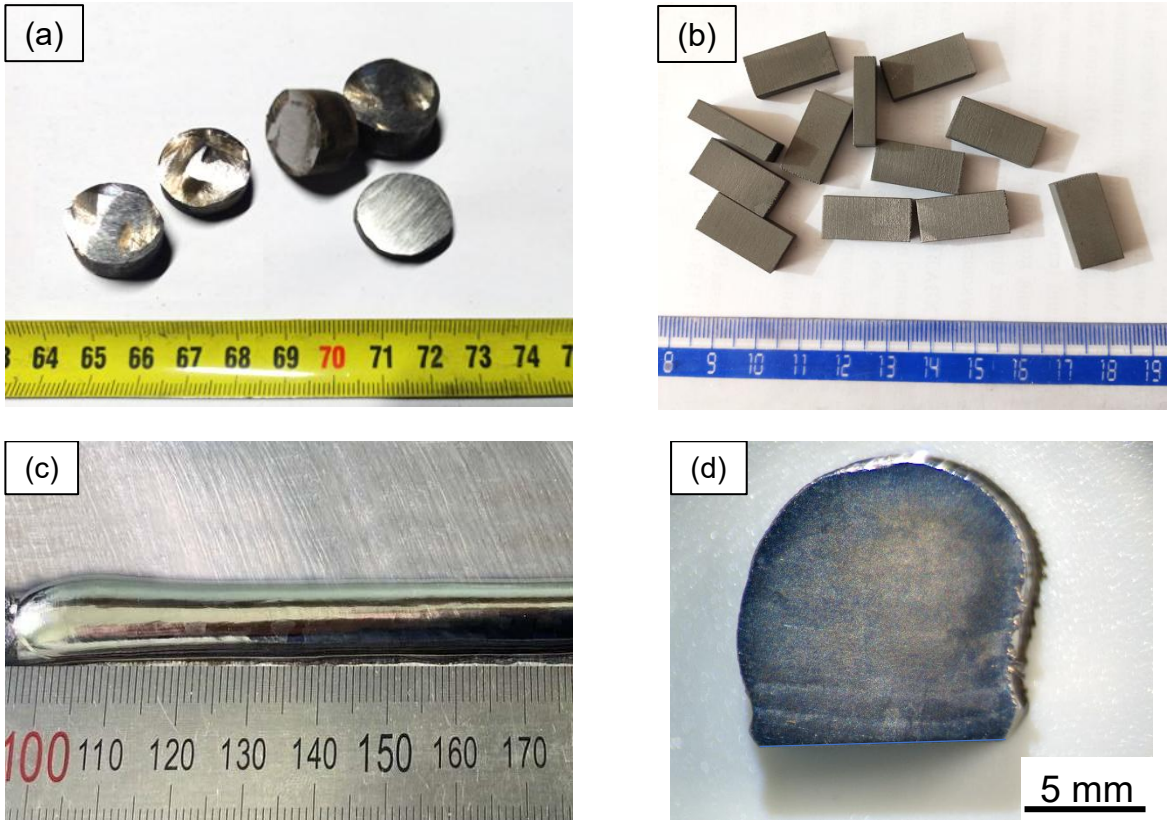


Fig. 1 The appearance of the Ti-6Al-4V alloy samples cut from the hot-rolled bar (a), and obtained by SLM (b), and WAAM (c, d)

The structural properties and microhardness of the Ti–6Al–4V alloy samples obtained by different methods were studied in the as-received state and after heat treatment. The marking of the samples, according to their manufacturing method and heat treatment regime, is provided in Table 2.

Standard grinding and polishing techniques were used to prepare the samples for the microstructural and microhardness studies. Etching was carried out using an aqueous solution of 2% HF + 2% HNO_3. The microstructure was analyzed using an optical metallographic microscope iScope IS.1053-PLMi. Microhardness was determined using the Vickers method with the LHVS-1000Z device, applying a load of 100 g and a dwell time of 10 seconds.

For X-ray diffraction analysis, a Rigaku Ultima IV diffractometer (Cu Kα radiation, λ = 1.5406 Å) was used, with an angular range of 2θ = 20°– 120°, a registration step of 0.04°, and an exposure time of 2 seconds at each point. The quantitative phase composition of the Ti-6Al-4V alloy was calculated based on the integrated intensities of non-overlapping diffraction maxima typical for each phase, using the Rietveld approach realized in the PDXL software. The phase composition was refined by fitting structural models of α-Ti (HCP, 194: $P6_3/mmc$) and β-Ti (BCC, 229: Im3m) from the Inorganic Crystal Structure Database (ICSD), along with refining scale factors, lattice parameters, diffraction maximum profiles, and background. The pseudo-Voigt profile function and polynomial background modeling were applied. Based on X-ray diffraction results, the quantitative phase composition, the size of the coherent scattering domains (CSD), and the degree of crystal lattice deformation (ε) were determined.

Table 2 Making of the Ti-6Al-4V alloy samples depending on manufacturing method and treatment route

Sample marking		Condition	Heat treatment
Hot-rolled	H-0	As-received	–
	H-1	Annealed	990±10 °C, 4 hours, furnace cooling
	H-2	Quenched	990±10 °C, 1 hour, water quenching
	H-3	Aged after quenching	990±10 °C, 1 hour, water quenching + 530 ±10 °C, 6 hours, air cooling
SLM	S-0	As-received	–
	S-1	Annealed	990±10 °C, 4 hours, furnace cooling
	S-2	Quenched	990±10 ºC, 1 hour, water quenching
	S-3	Aged after quenching	990±10 °C, 1 hour, water quenching + 530 ±10 °C, 6 hours, air cooling
WAAM	W-0	As-received	–
	W-1	Annealed	990±10 °C, 4 hours, furnace cooling
	W-2	Quenched	990±10 °C, 1 hour, water quenching
	W-3	Aged after quenching	990±10 °C 6 hours, air cooling

3 Results and discussion

3.1 Microstructural study

At the first stage, microstructural study of the Ti–6Al–4V alloy samples obtained by various methods in their as-received state (H-0, S-0, and W-0) was carried out (fig. 2).

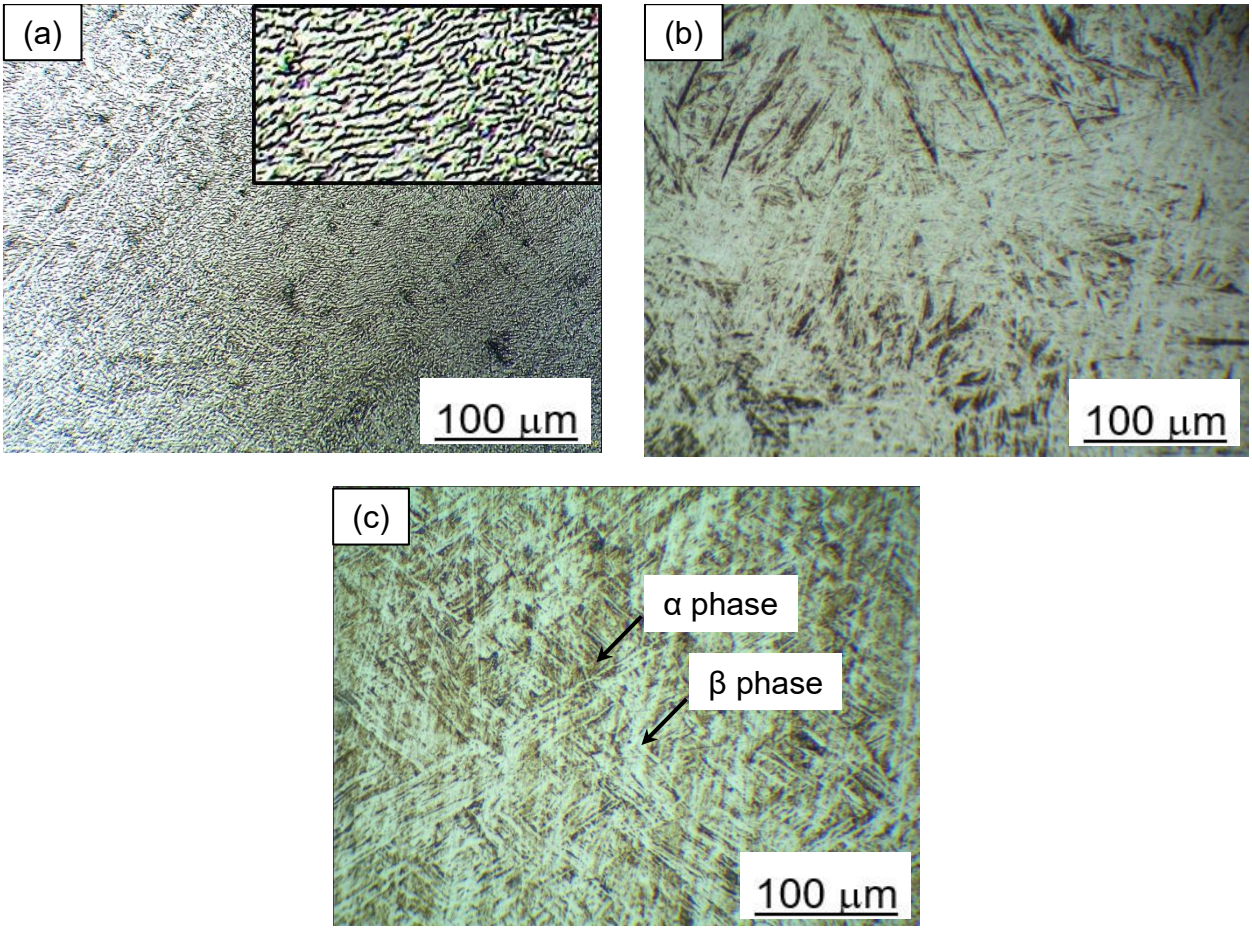


Fig. 2 Microstructure of the Ti–6Al–4V alloy obtained by different methods in the as-received state: hot-rolled sample H-0 (a); SLM sample S-0 (b); and WAAM sample W-0 (c). Magnification ×500

In the as-received state, the H-0 sample exhibits a fine-grained structure with a visible deformation texture. The grain sizes are 20 μm in length and 1 – 2 μm in width (fig. 1, a). This structure indicates a high degree of metal deformation, which affects subsequent structural modification during the following heat treatment, in particular, the acceleration of recrystallization processes.

Microstructure of the S-0 sample, obtained by SLM printing (fig. 2, b), is ununiform with needle-like grains of different sizes. Boundaries of macrograins are not clear enough to be recognized and micrograins are predominantly elongated, have a thin 20 – 100 μm plates of the α-phase. Such structure is markedly non-equilibrium and approaches to the structure of a hardened-like state.

The W-0 sample, obtained by the WAAM method, in the as-received state reveals a structure more similar to obtained for H-0 sample, which contains homogeneous α-phase colonies of uniform size with plates whose length does not exceed 20 – 30 μm and width of ~1 μm. Unlike the S-0 sample, no noticeable structural heterogeneities or gas shrinkage defects in the form of pores were observed.

The microstructure of the Ti-6Al-4V alloy after annealing, shown in Fig. 3, indicates similarities in structural modification between the hot-rolled H-1 and the SLM S-1 samples. This fact can be partially attributed to the initial fine-grained microstructure, observed for the H-0 and W-0 samples. Such structure enhances recrystallization processes, allowing the microstructure to quickly reorganize and modify uniformly. In both cases, it is characterized by distinct α-phase plates and β-phase located in the interphase regions. The β-phase appears to be less prominent in the SLM sample S-1. At the same time, this sample contains α-phase colonies, and the plates are smaller, with sizes ranging from 10 to 100 μm. This sample has more defects, which may indicate a higher oxygen saturation and, consequently, a higher degree of α-phase stabilization.

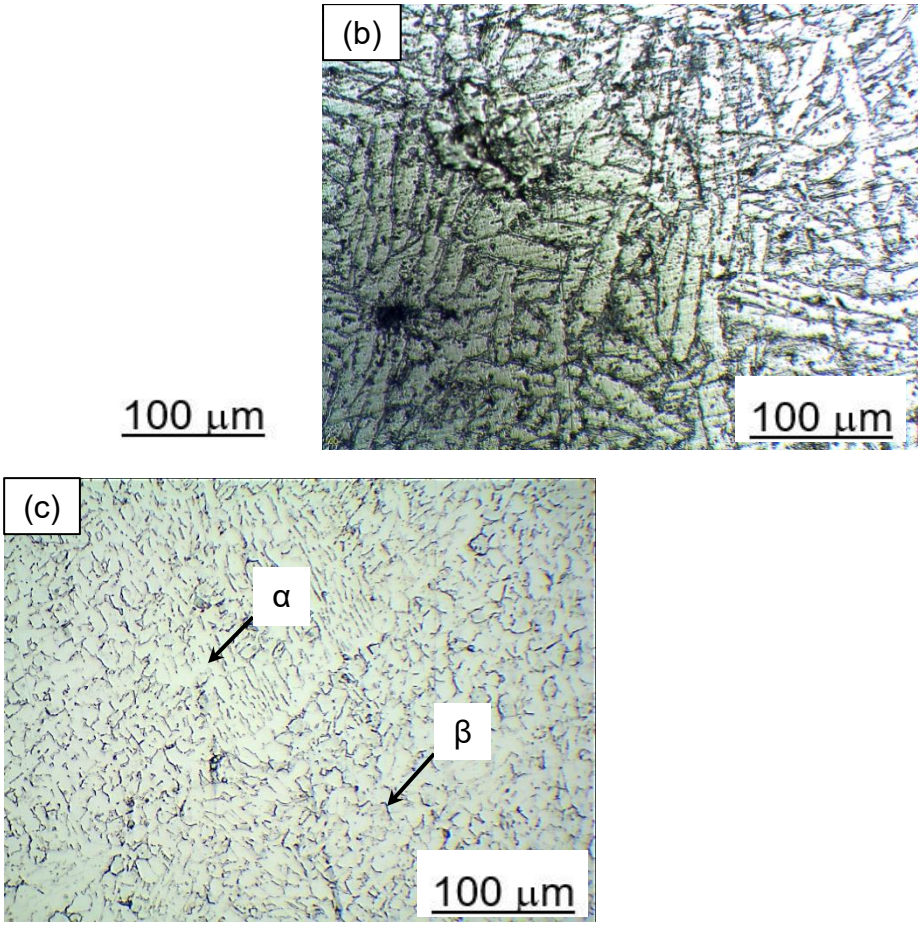


Fig. 3 Microstructure of the annealed Ti–6Al–4V alloy obtained by different methods: hot-rolled sample H-1 (a); SLM sample S-1 (b); and WAAM sample W-1 (c). Magnification ×500

For the M-1 and S-1 samples, the length and thickness of the α-phase plates are 20 – 200 μm and 5 – 15 μm, respectively. There are almost no clear colonies of α-phase

plates, and the structure of the samples generally corresponds to the standard for the studied alloy in the annealed state.

The W-1 sample reveals a structure several times finer compared to other two studied samples after the same heat treatment. Additionally, it contains small globular grains, which are not typical for the annealed state. This fact can be attributed to the higher time needed for recrystallization of WAAM produced Ti–6Al–4V alloy compared to the samples fabricated by other methods.

After quenching, all three studied samples exhibit signs of a martensitic-like structure (fig. 4). The hot-rolled H-2 sample reveals the most homogeneous structure with the shortest α'-phase length of ~30 μm. The S-2 sample, obtained by SLM printing, has a coarser microstructure after quenching and is characterized by lower etching resistance. The α'-phase is predominantly large with sizes ranging from 80 to 100 μm. Quenching of the WAAM sample results in an inhomogeneous structure, where the α'-phase is represented by needles of various sizes, ranging from 20 to 130 μm.

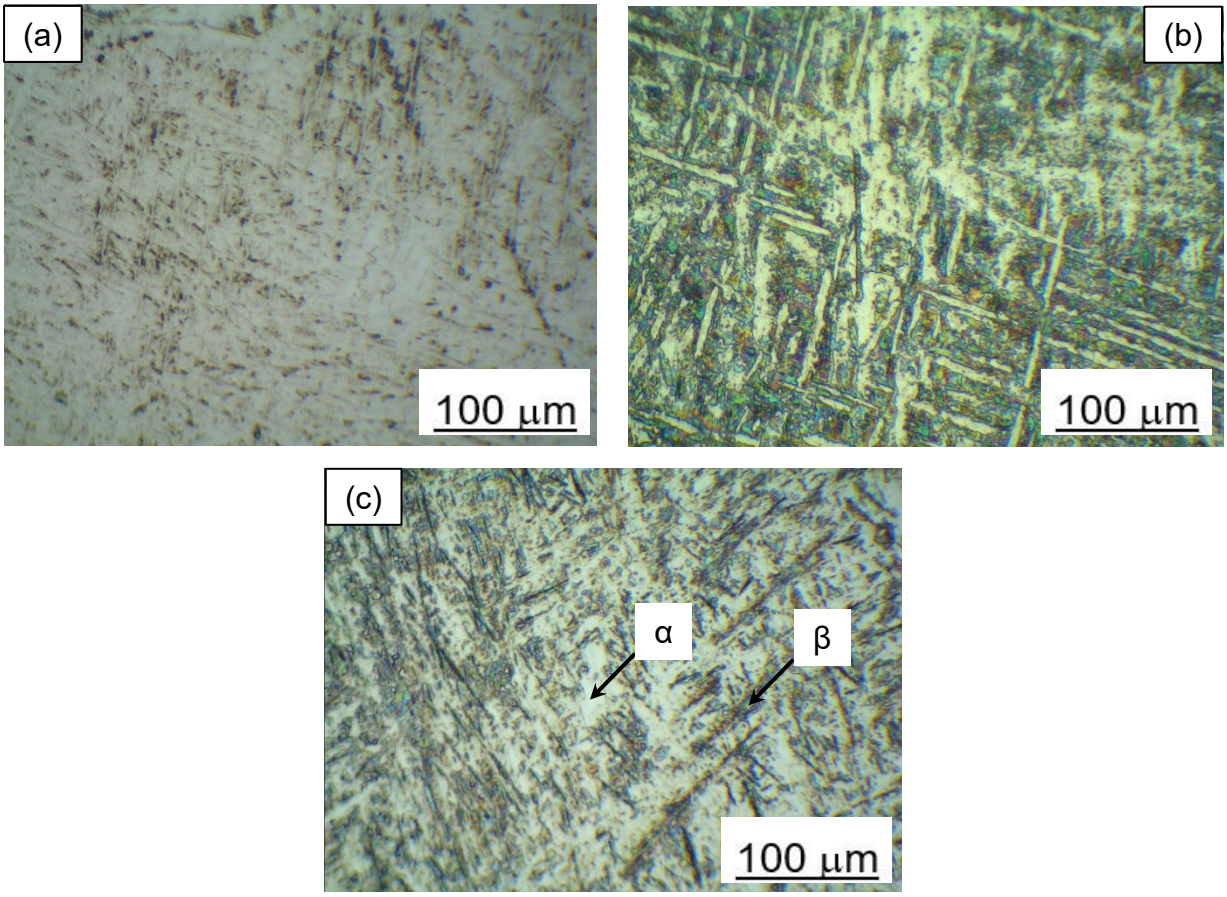


Fig. 4 Microstructure of the quenched Ti–6Al–4V alloy obtained by different methods: hot-rolled sample H-2 (a); SLM sample S-2 (b); and WAAM sample W-2 (c). Magnification ×500

Further aging affects the final structure (fig. 5) of the samples in different ways, depending on the structural features formed after quenching. In the hot-rolled H-3 sample, the α'-phase noticeably coarsens. For the S-3 sample, aging after quenching induces similar but more pronounced structural changes, making it difficult to distinguish the α-

and α’-phases. Such an atypical pattern for an aged sample may be explained by the so-called 'microstructural instability' which manifests above 450 °C and is typical for Grade 5 alloy produced by the SLM method [30]. The microstructure of the W-3 sample after aging is the most favorable, as a significant amount of the fine-disperse α’-phase is preserved.

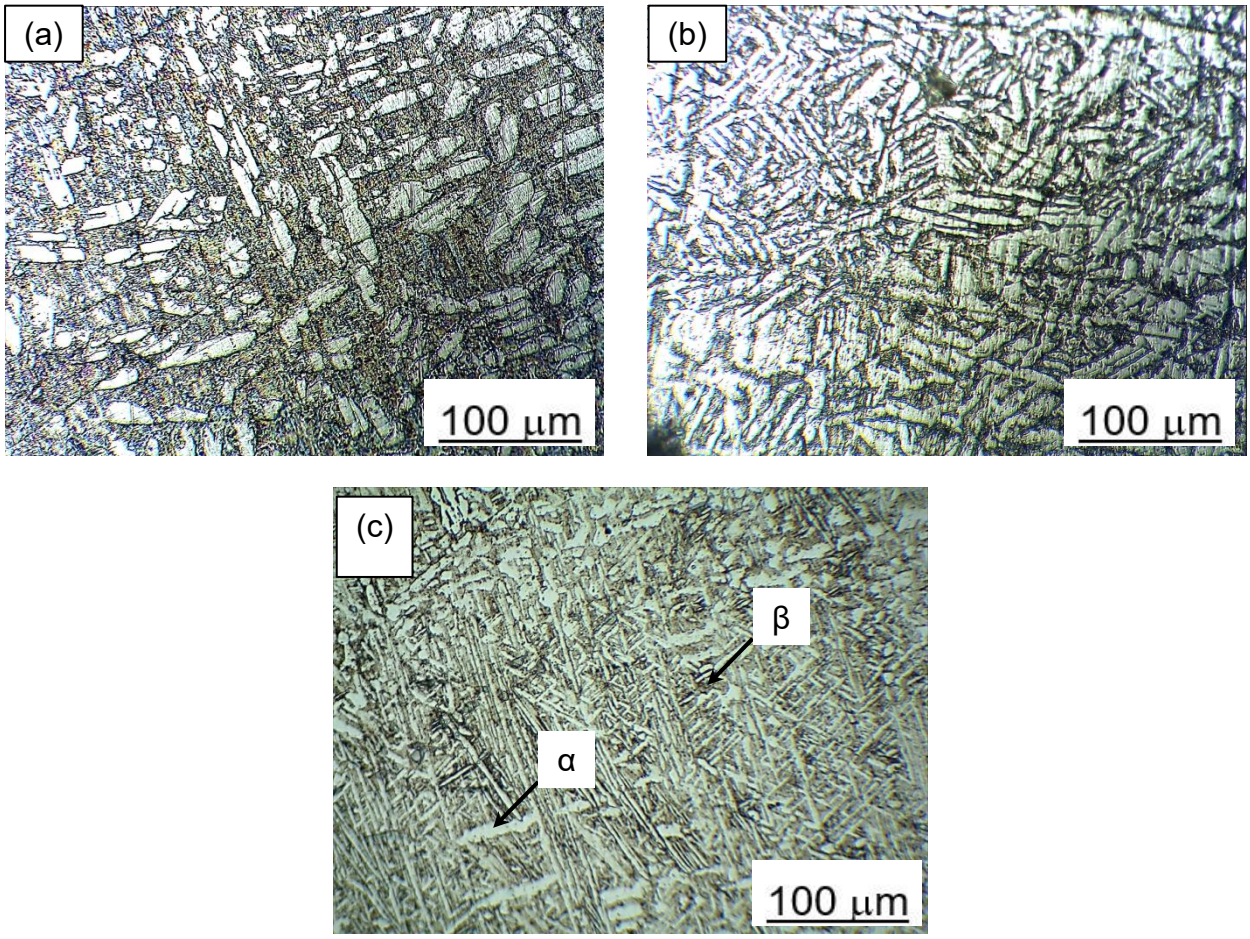


Fig. 5 Microstructure of the quenched and subsequently aged Ti–6Al–4V alloy obtained by different methods: hot-rolled sample H-3 (a); SLM sample S-3 (b); and WAAM sample W-3 (c). Magnification ×500

Thus, the alloy production method drastically affects the microstructure of the Ti–6Al–4V alloy in both as-received and heat-treated states. The most notable differences in microstructure were observed for the samples after the quenching with the following aging.

3.2 Microhardness analysis

The effect of the microstructure formed as a result of various fabrication methods and treatment routes on the microhardness of the examined samples is shown in Fig. 6.

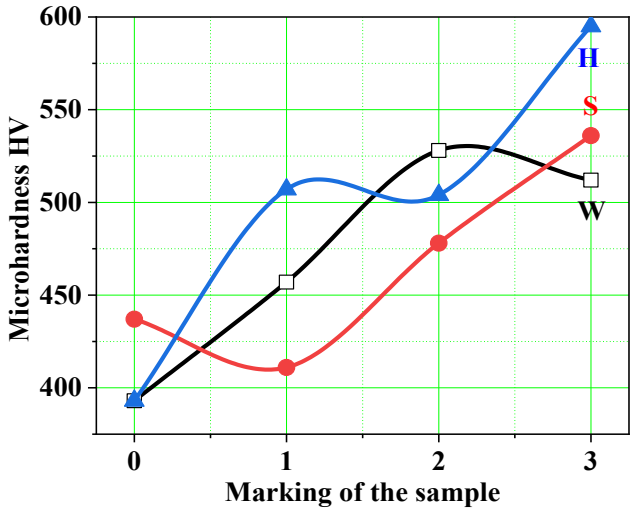


Fig. 6 Microhardness of Ti–6Al–4V alloy fabricated by various methods and treated by different regimes

The highest microhardness in the as-received state is attributed to the sample obtained via SLM method (437 HV). For the S-0 sample, a higher saturation with gas impurities is evident, which further stabilizes the α-phase and results in higher microhardness [31]. For this sample, an expected dependence of microhardness on the heat treatment conditions was also observed. It consists of a specific decrease in hardness after annealing (411 HV), an increase after quenching (478 HV), and an additional increase after aging (536 HV).

For the samples obtained by WAAM and conventual methods, the microhardness values in the as-received state are practically the same (~393 HV). Although the microstructure of the hot-rolled sample is more typical for a cast state, and of the WAAM sample – for a deformed one, both are equally fine-grained, leading to close microhardness. Additionally, the similar microhardness of these samples indicates a low content of gas impurities in the WAAM alloy. After annealing, the microhardness increases due to recrystallization processes. For the H-1 sample, the microhardness increases to 457 HV, and for the W-1, it rises to 507 HV.

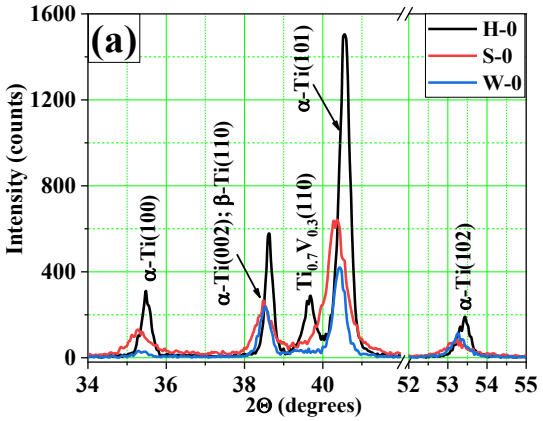
The aging of the quenched hot-rolled sample results in a decrease in microhardness down to 512 HV. Considering that the microstructure of this sample is relatively coarse (the α'-phase coarsens), this may indicate an effect similar to observed during annealing, where excess stresses in the initial structure promote an acceleration of diffusion and recrystallization processes. The microhardness of the W-3 sample after aging is expectedly increased to 595 HV.

As a result of quenching and aging, the highest microhardness of 595 HV was achieved for the W-3 sample, the middle value of 536 HV – for the S-3 sample, and the lowest value of 512 HV – for the H-3 one. This result indicates that AM enables an increase in the microhardness of Ti-6Al-4V alloy products, both in the as-received state (SLM) and after heat treatment (WAAM), compared to metallurgical production.

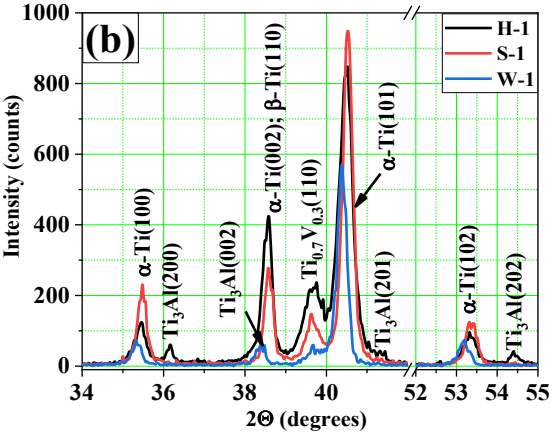
3.3 Phase composition analysis

The interdependence of microstructure and microhardness of Ti–6Al–4V alloy cannot be interpreted unambiguously. To gain a more comprehensive understanding of

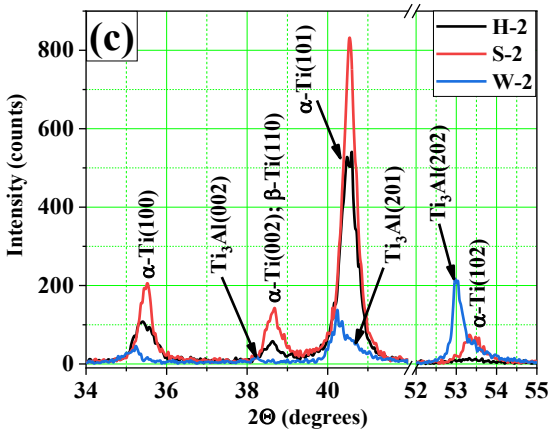
the structural and phase transitions, X-ray diffraction studies were conducted, the results of which are presented in Fig. 7 and Fig. 8.



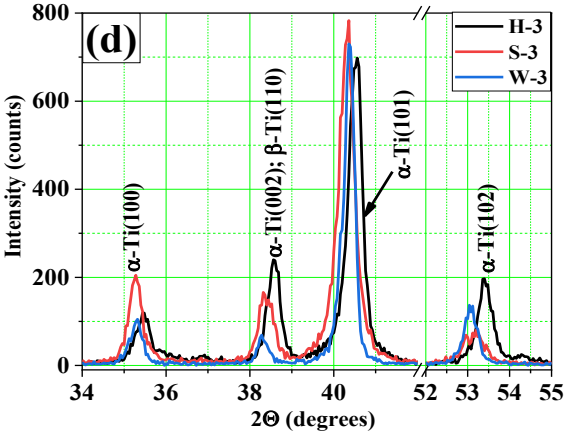
Phase	Sample		
	H	S	W
α-Ti	63	85	78
β-Ti	10	15	22
$Ti_{0.7}V_{0.3}$	27	–	–



Phase	Sample		
	H	S	W
α-Ti	75	83	91
β-Ti	14	9	2
Ti_3Al	2	–	–
$Ti_{0.7}V_{0.3}$	9	8	7



Phase	Sample		
	H	S	W
α-Ti	68	57	70
β-Ti	32	43	25
Ti_3Al	–	–	5



Phase	Sample		
	H	S	W
α-Ti	88	97	94
β-Ti	12	3	6

Fig. 7 Diffraction patterns and quantitative phase composition of the Ti–6Al–4V alloy, obtained by different methods: as-received (a), annealed (b), quenched (c) and aged after quenching (d)

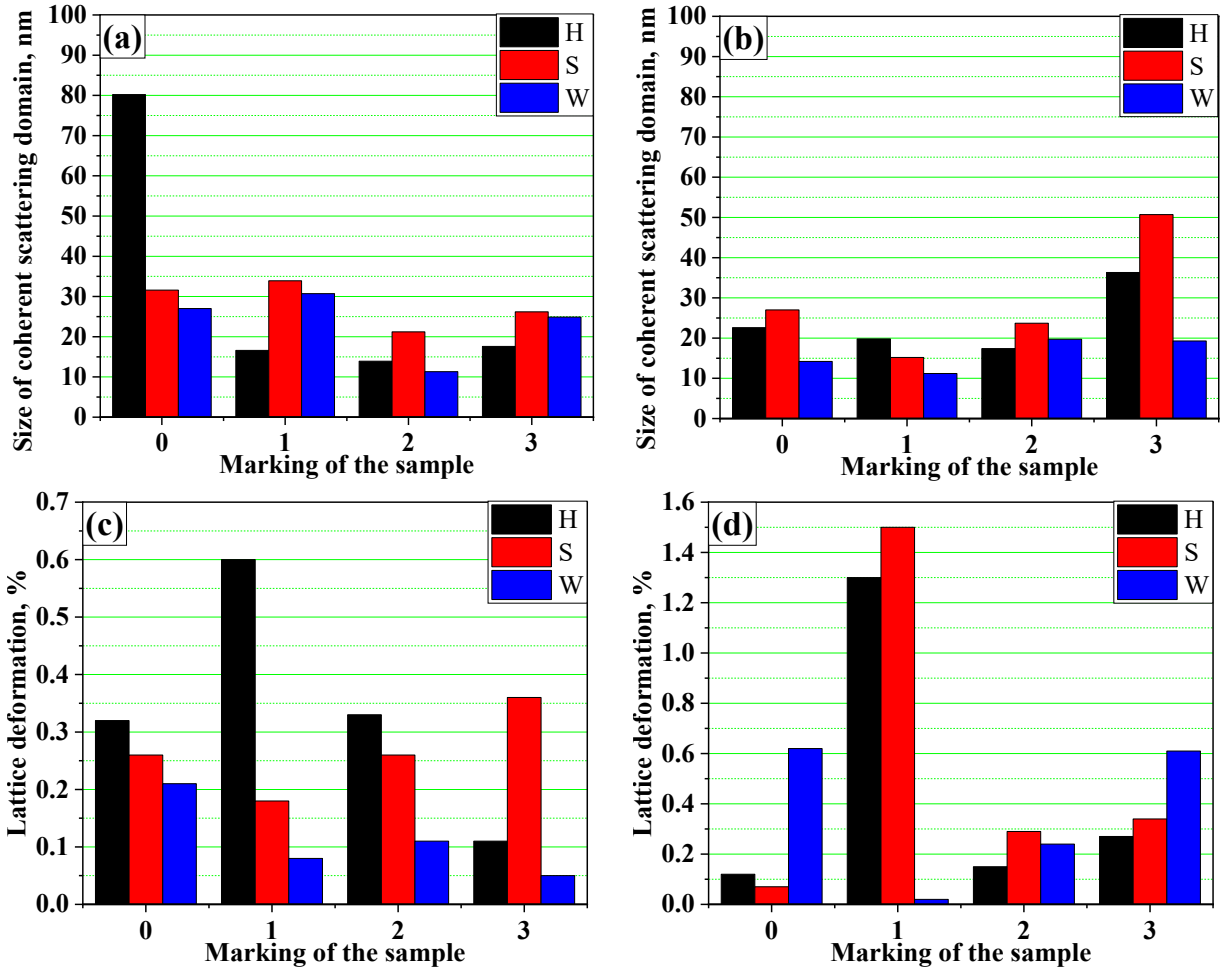


Fig. 8 Structural properties of the α-Ti (a, c) and β-Ti (b, d): a, b – size of coherent scattering domains and c, d – lattice deformation

Ti-6Al-4V alloy *α→β* phase transformation significantly depends on the heating temperature and cooling rate [32]. Thus, the phase transformations occurred during 3D printing, providing extremely high crystallization rate, can differ markedly from the metallurgical processes.

Diffraction patterns of all samples in the as-received state (Fig. 7, a), regardless of the preparation method, display diffraction peaks corresponding to the hexagonal α-phase and the cubic β-phase (the most intense peak from the β-phase (110) partially overlaps with the diffraction maximum (002) from the α-phase).

For the Ti-6Al-4V alloy obtained by conventual method (H-0), diffraction peaks corresponding to the $Ti_{0.7}V_{0.3}$ solid solution were also observed, indicating the presence of V in the crystal lattice of the β-phase. For this sample, the intensity of the diffraction maxima from the α-phase, particularly (101), is the highest, suggesting a low degree of defectiveness and an equilibrium two-phase α+β structure.

Unlike the H-0 sample, the diffraction patterns of the Ti-6Al-4V alloy obtained via SLM technology (S-0) show exclusively diffraction maxima from the α- and β-phases. This fact is caused by the extremely high cooling rate during the SLM process (up to

10^6 °C/s), which stabilize the high-temperature β-phase, preventing its transformation into the equilibrium α-phase [33].

Diffraction patterns of the Ti-6Al-4V alloy obtained by WAAM technology (W-0) reveal the lowest intensity of diffraction maxima from the α-phase. The α-phase diffraction peaks from this sample exhibit a smaller full width at half maximum compared to the S-0 sample, indicating the presence of a coarse-grained structure, macroscopic texture, and internal heterogeneity caused by the cyclic nature of the solidification and the complex thermal history of layer-by-layer deposition, including reheating, remelting, and recrystallization of local regions within the sample, as opposed to the SLM process.

The lower cooling rate during the WAAM process, compared to SLM, also promotes formation of a higher β-phase amount (Fig. 8). [20, 34].

A certain difference in the results of microstructural (Fig. 2, b) and X-ray diffraction analysis can be explained by the fact that, during WAAM, each layer cools differently, manifesting in the formation of local textures and microdeformations, leading to an uneven contribution of the samples different areas to the overall diffraction signal.

Thus, the phase composition of the Ti-6Al-4V alloy significantly depends on the manufacturing technology (Fig. 8). After hot rolling (H-0), a stable structure with a predominance of the α-phase (63 wt.%) is observed. The SLM sample (S-0) is characterized by the highest α-phase content (85 wt.%), which requires further heat treatment to stabilize the structure. The WAAM sample (W-0) has the α-phase content of 78 wt.% and the least crystalline order, necessitating optimization of the heat treatment conditions.

The highest content of the α-phase (85 wt.%) is observed for the S-0 sample, which also reveals the highest microhardness (437 HV). However, the lowest content of the α-phase in the H-0 sample (63 wt.%) does not significantly reduce its microhardness value, which remains practically the same compared to the W-0 sample (393 HV). This result can be explained by the fine-grained structure, which influences the formation of transitional areas at the boundaries between the α- and β-phases, identified as $Ti_{0.7}V_{0.3}$.

The amount of the $Ti_{0.7}V_{0.3}$ phase reaches 27 wt.% for the H-0 sample. The CSD sizes for the W-0 sample (27 nm for the α-phase and 31.6 nm for the β-phase) are smaller compared to the H-0 sample (80.2 nm and 22.6 nm, respectively).

For the AM manufactured samples, a shift and broadening of all diffraction peaks were observed. This effect is more pronounced for the α-phase of the S-0 sample, indicating residual stresses and a fine-grained martensitic α'-structure that does not have enough time to relax [33]. The lattice deformation (ε) of the β-phase is highest for the W-0 sample, reaching the value of 0.62%. A large amount of β-phase (22 wt.% compared to 10 wt.% for the H-0 sample) has to undergo more than one stage of structural reorganization, which can be roughly expressed in the following sequence: reduction of stresses, decay and dispersion of α'-phase, its further growth and transformation into the α-phase, reorganization into the β-phase, brief growth of the β-phase, and subsequent phase recrystallization. This process is likely not fully complete, as evidenced by the shift in diffraction maxima for the annealed W-1 sample.

Fig. 7, b shows the diffraction patterns of the Ti–6Al–4V alloy after annealing at 990 °C for 4 hours. This annealing temperature exceeds the eutectoid transformation temperature (~975 °C), which ensures complete or partial transformation of the α-phase into the high-temperature β-phase, followed by the decomposition during cooling.

Typical diffraction maxima corresponding to the α-phase, β-phase, and Ti_3Al intermetallic were registered in all investigated cases. The presence of diffraction maxima from the β-phase and $Ti_{0.7}V_{0.3}$ indicates the retention of residual β-phase or the formation of stabilized impurity structures as a result of slow cooling after annealing. The presence of the Ti_3Al phase is a consequence of the decomposition of a supersaturated solid solution following high-temperature heating [34].

Diffraction patterns of the H-1 sample reveal a significant decrease in the intensity of the maxima from the α-phase, compared to the as-received state (H-0) as well as appearance of peaks from the intermetallic Ti_3Al. This result indicates a substantial enrichment of the α-phase with Al during high-temperature stabilization and subsequent cooling. The β-phase content increases to 14 wt.%.

In the diffraction patterns of the S-1 sample, the highest intensity of the (101) peak from the α-phase was observed, indicating significant recrystallization growth of α-phase grains during annealing. After such treatment, the sizes of the microstructural elements become more uniform; however, secondary phases such as Ti_3Al were also formed, which is in agreement with the results reported in [35].

The diffraction patterns of the W-1 sample reveal the lowest overall intensity of diffraction maxima, which may indicate the formation of a coarse-grained columnar structure, reducing the number of grains capable of diffracting in specific orientations [36].

The difference between microstructural (fig. 3, b) and X-ray diffraction analysis results compared to the as-received state (W-0) is explained by the characteristic features of the thermal processes that occur during the formation of the materials layered structure in the WAAM process.

Peaks from the intermetallic Ti_3Al are present; however, they exhibit the lowest intensity. The relatively slow cooling rate of WAAM, combined with repeated thermal cycling during layer-by-layer deposition, contribute to the stabilization and growth of the α-phase. Such thermal conditions also lead to partial reduction of structural defects. Nevertheless, despite the prolonged thermal exposure, the total holding at temperatures sufficient for active diffusion remains limited within each cycle. As a result, diffusion-controlled precipitation of secondary intermetallic phases, including Ti_3Al, does not fully complete, which explains their low volume fraction and weak diffraction intensity.

For all processing routes, the change in the β-phase content is primarily caused by differences in the thermal exposure and the kinetics of phase transformations. In the S-1 and W-1 samples, a noticeable decrease in the amount of β-phase is observed, while for the H-1 sample the β-phase fraction slightly increases due to the reduction of the transitional $Ti_{0.7}V_{0.3}$ phase. Additionally, the formation of a small amount (≈2 wt.%) of the ordered α_2-Ti_3Al phase is detected for the H-1 sample.

In additively manufactured materials, longer times are required to reach an equilibrium phase state. As a result, the β-phase content remains lower (9 wt.% for S-1 and 2 wt.% for W-1) compared with the H-1 sample (14 wt.%). At the same time, the amount of the $Ti_{0.7}V_{0.3}$ transitional phase (7–8 wt.%) is comparable to that of the H-1 sample (9 wt.%). The deformation degree of the crystal lattice increases for all phases of the H-1 sample after annealing, especially for the β-phase (from 0.12% for M-0 to 1.3% for M-1). For the W-1 sample, on the contrary, the ε values decrease compared to the as-received state: from 0.21% (W-0) to 0.08% (W-1) for the α-phase and from 0.62% (W-0) to 0.02% (W-1) for the β-phase. For the S-1 sample, the ε values for the α-phase also

decrease compared to the initial state (from 0.26% to 0.18%), although not as significantly as for the W-1 sample; however, the deformation degree of β-phase crystal lattice increases (from 0.07% to 1.5%).

Regarding the size of the CSD, no significant changes occur except for the α-phase of the S-1 sample, for which this value extremely decreases (from 80.2 nm to 16.6 nm).

Changes in the α-phase content and the deformation degree of its crystal lattice affect the magnitude of the microhardness. After annealing, the microhardness of the H-1 sample increases from 393 HV to 457 HV, meaning the strengthening effect of 16% (fig. 6). On the other hand, for the S-1 sample, the microhardness decreases by ~5%. This effect can be attributed to the reduction in the deformation degree of the α-phase crystal lattice from 0.26% to 0.18% as well as a slight decrease in its content (fig. 7). Additionally, the layered hardened structure with a high dislocation density, formed as a result of the high cooling rate typical for the SLM method, is destroyed.

Annealing of the WAAM sample (W-1) results in the most significant increase in microhardness – from 393 HV to 507 HV, indicating a strengthening effect of ~30%. This result can be explained by the fact that annealing activates the transformation of the β-phase into the α-phase, resulting in martensitic strengthening due to the formation of a fine α-phase plate structure (fig. 3, b). The significantly finer structure of the W-1 sample compared to the H-1 and S-1, in the form of globular grains, also contributes to the strengthening.

Fig. 7, c shows the diffraction patterns of the Ti–6Al–4V alloy after annealing at 990 °C for 1 hour, followed by water quenching. This thermal regime ensures a complete transformation of the α-phase into the β-phase during heating, while the rapid cooling allows to fix metastable structures or preserve a supersaturated solid solution.

The diffraction patterns of the H-2 and S-2 samples contain typical peaks from the α-phase. For the W-2 sample, a completely different diffraction patterns were observed with the intense peaks from the intermetallic Ti_3Al phase.

Diffraction peaks from $Ti_{0.7}V_{0.3}$, which were present at the spectra of the annealed samples, were not observed, indicating dissolution of this phase in the β-solid solution. Without prolonged holding at low temperatures the phase equilibrium shifts and V fully returns to the β-solid solution, stabilizing it.

For the H-2 sample, a decrease in the peaks from the α-phase intensity compared to the annealed state was observed; while peaks from $Ti_{0.7}V_{0.3}$ and Ti_3Al were not identified. At the same time, the reduction in the intensity of the peaks from the α-phase, compared to H-1, indicates a partial transformation of the α-phase [36].

The diffraction patterns of the S-2 sample reveal the highest intensity of the (101) peak from the α-phase, which may be related to the grains texture and recrystallization typical for rapidly cooled additively manufactured structures.

For the W-2 sample, a reduced intensity of the diffraction maxima from the α-phase was observed; however, this reduction is associated with finer grains, increased microstructural homogeneity, and a lower degree of preferred crystallographic orientation rather than a decrease in the α-phase fraction. Such diffraction behavior may originate from the specific thermal cycling experienced by each deposited layer, which promotes grain refinement and reduces the texture. Additionally, slight surface oxidation could

contribute to partial stabilization of the α-phase during thermal exposure, preserving its dominant fraction even after quenching [20].

The most significant β-phase amount was observed for the SLM sample (S-2), which can be attributed to the high cooling rate during printing (>10^5–10^6 °C/s), a supersaturated structure formation, and insufficient diffusion for the complete decomposition of the β-phase even during heat treatment. Additionally, the SLM process is characterized by local chemical heterogeneity (the melting zone is enriched with β-stabilizers – V, Mo), which locally increases the stability of the β-phase and partially blocks the complete transition to the α-phase even during quenching.

The WAAM process has a moderate cooling rate (10 – 100 °C/s) compared to SLM, and provides more time for the β → α transformation during cooling and quenching, which explains the significantly lower amount of β-phase in the W-2 sample compared to the S-2.

The changes in the quantitative phase composition and the crystallographic parameters after quenching affect the microhardness differently, determining the strengthening mechanisms specific to the production route of the Ti–6Al–4V alloy. Quenching of the hot-rolled sample (H-2) results in an additional increase in microhardness of ~15% compared to its annealed state (H-1) and ~35% relative to the initial state (H-0).

Hardening of the SLM sample (S-2), similar to the H-2 case, results in the microhardness increase (fig. 8); however, the nature of this change compared to the as-received state (S-0) is different. After hardening (S-2), the microhardness increases by ~15% compared to the annealed state (S-1) and only by ~9% compared to the as-received one (S-0). The increase in microhardness is attributed to a reduction in the size of the α- and β-phase CSD by ~1.5 times (fig. 8), as well as an increase in the deformation degree of the α-phase crystal lattice from 0.18% to 0.26%.

For the WAAM sample (W-2), the microhardness after quenching remains practically unchanged. This effect can be explained by the fact that although the size of the α-phase CSD after quenching (W-2) decreases by ~2.5 times, the degree of the lattice deformation does not undergo significant changes, and the α-phase content decreases from 91% to 70%.

According to microstructural study (fig. 4), after quenching, signs of a martensitic-like structure appear in all three types of the investigated samples. However, it is practically impossible to distinguish diffraction peaks from the α-phase HCP lattice and the α'-martensite due to similar lattice parameters of these phases. The formation of martensite during quenching and its morphology also affect the microhardness.

Figure 7, d shows the diffraction patterns of the Ti–6Al–4V alloy after quenching at 990 °C for 1 hour, followed by artificial aging at 530 °C for 6 hours. This treatment aims to stabilize the structure, reduce residual stresses, and form dispersed strengthening phases.

For all three states (H-3, S-3, W-3), predominantly α-phase peaks were observed. The shift of the α-phase diffraction maxima towards smaller angles for the Ti-6Al-4V alloy obtained by SLM and WAAM technologies may confirm the formation of martensitic α’-phase, which was visually observed by microstructural study (fig. 5).

In the H-3 sample, X-ray diffraction analysis revealed a two-phase structure with a well-ordered α-phase. The increased intensity of the (101) and (002) peaks from α-phase reflects the presence of a preferred crystallographic orientation formed during slow cooling. However, this texture is less pronounced compared to the deformation-induced rolling texture in the as-received state (H-0) and weaker compared to the texture partially retained after annealing (H-1) [34].

For the SLM sample (S-3), the higher intensity of the α-phase diffraction peaks compared to the hot-rolled sample (H-3) indicates a more ordered α-phase structure and partial recrystallization occurring during aging. This behavior may also reflect the higher sensitivity of the SLM-produced microstructure to oxygen-induced stabilization of the α-phase. The minimal fraction of the β-phase (fig. 8) further confirms the effectiveness of the heat treatment in stabilizing the α-dominated structure formed during the rapid cooling characteristic of the SLM process [35-38].

For the WAAM sample (W-3), the intensity of the peaks also indicates a stable two-phase structure with a well-ordered α-phase, similar to the H-3 sample. The increase in the intensity of (101) diffraction maximum from the α-phase compared to (002) suggests the preservation of residual texture, which is associated with directional heat transfer during the WAAM process [20].

After aging, the intensity of the (101) diffraction maximum from the α-phase is almost the same for different preparation methods. Still, the shift of this peak towards smaller angles for the AM samples remains more noticeable compared to the hot-rolled one. The most pronounced shift and broadening of the diffraction peaks were observed for the S-3 sample, which likely indicates the formation of the most considerable amount of martensitic α’-phase and is confirmed by the microstructural analysis (fig. 5, b).

The application of aging after quenching of the Ti–6Al–4V alloy, regardless of the manufacturing technology, is accompanied by a significant reduction in the β-phase amount (fig. 8). The decrease in β-phase content in the AM Ti-6Al-4V alloy is a critical factor influencing the increase in microhardness. Thus, aging after quenching of the S-3 sample results in an additional rise in microhardness by 12%, while for the W-3 sample it is 18%. For the H-3 sample, the β-phase content is 2 – 4 times higher compared to the other samples, resulting in the lowest microhardness.

The size of the α-phase CSD after aging does not undergo significant changes compared to quenching. The size of the β-phase CSD for the H-3 and S-3 samples increases twofold after aging. At the same time, the degree of the crystal lattice deformation decreases by 2-3 times for all samples.

According to X-ray diffraction study of the Ti–6Al–4V alloy after quenching and subsequent aging, it can be concluded that the main factor contributing to the increase in the microhardness of the Ti–6Al–4V alloy received by AM methods is the reduction in the β-phase amount and the formation of α’-martensite. The morphology of the α’-martensite also influences the microhardness – the presence of fine-dispersed needle-like martensite in the sample W-3 (fig. 5, c) results in a higher microhardness compared to the S-3 sample (fig. 6, b).

4 Conclusions

In this work, the microstructure, microhardness, and phase composition of the as-received and heat-treated Ti-6Al-4V alloy produced by additive manufacturing and conventional metallurgical routes were investigated. It was found that fabrication method significantly influences the structural evolution of the alloy during heat treatment, leading to differences in the morphology and volume fractions of the α and β phases. These microstructural variations are directly reflected in the resulting microhardness, indicating distinct phase transformation and stabilization behaviors for the compared processing routes.

The optimal heat treatment regime of the Ti-6Al-4V alloy, obtained by metallurgical method, is an annealing at 990 °C for 1 hour, followed by quenching in water. This treatment route allows to achieve a maximum microhardness of 528 HV.

The optimal heat treatment mode of the Ti-6Al-4V alloy, obtained through additive technologies such as SLM and WAAM, is a quenching at 990°C for 1 hour, followed by artificial aging at 530°C for 6 hours. This heat treatment regime ensures the formation of α'-martensite and the most significant degree of lattice deformation with a corresponding maximum increase in microhardness.

The WAAM technology leads to a higher microhardness after quenching with subsequent aging compared to SLM technology due to the formation of fine-disperse, needle-shaped martensite. The microhardness values of the aged WAAM and SLM samples are 595 HV and 536 HV, respectively.

Additive manufacturing, compared to the metallurgical methods, allows to increase the microhardness of Ti-6Al-4V alloy products both in the as-received state (the microhardness of the as-received SLM sample is 437 HV compared to 393 HV of initial hot-rolled sample), and after heat treatment (the microhardness of the aged WAAM sample is 595 HV compared to 512 HV for the aged hot-rolled sample).

Author contributions

Conceptualization: Andrii Burmak, Svitlana Voloshko, Mykhailo Voron, Serhiy Schwab, Igor Vladymyrskyi; Methodology: Andrii Burmak, Svitlana Voloshko, Serhiy Schwab, Ievgen Byba; Formal analysis and investigation: Andrii Burmak, Mykhailo Voron, Ievgen Byba; Writing – original draft preparation: Andrii Burmak, Svitlana Voloshko, Mykhailo Voron, Serhiy Schwab; Writing – review and editing: Svitlana Voloshko, Igor Vladymyrskyi; Resources: Andrii Burmak, Svitlana Voloshko, Serhiy Schwab; Supervision: Svitlana Voloshko, Igor Vladymyrskyi; Funding acquisition – Svitlana Voloshko.

Acknowledgements

The work was supported by the Ministry of Education and Science of Ukraine under the Project #0124U001001.

The authors acknowledge the E.O. Paton Institute of Electric Welding of the National Academy of Sciences of Ukraine for providing facilities and technical support for the layer-by-layer wire arc additive manufacturing process used for the samples fabrication.

Data availability

Data is available upon request.

Declarations

Competing of Interest The authors declare no competing interests.

References

1. Marks, P. (2011). 3D printing takes off with the world's first printed plane. New Scientist, 211(2823), 17–18. https://doi.org/10.1016/s0262-4079(11)61817-4
2. Ashley, S (1995). Rapid prototyping is coming of age. Mechanical Engineering, 117(7).
3. Xu, W. (2022). Direct Additive Manufacturing Techniques for Metal Parts: SLM, EBM, Laser Metal Deposition. 290–318. https://doi.org/10.1016/b978-0-12-819726-4.00095-8
4. Edgar, J., & Tint, S. (2015). "Additive Manufacturing Technologies: 3D Printing, Rapid Prototyping, and Direct Digital Manufacturing", 2nd Edition. Johnson Matthey Technology Review, 59(3), 193–198. https://doi.org/10.1595/205651315x688406
5. Zhang, Y., Wu, L., Guo, X., Kane, S., Deng, Y., Jung, Y.-G., Lee, J.-H., & Zhang, J. (2017). Additive Manufacturing of Metallic Materials: A Review. Journal of Materials Engineering and Performance, 27(1), 1–13. https://doi.org/10.1007/s11665-017-2747-y
6. Hu, Y., Chen, H., Jia, X., Liang, X., & Lei, J. (2022). Heat treatment of titanium manufactured by selective laser melting: Microstructure and tensile properties. Journal of Materials Research and Technology, 18, 245–254. https://doi.org/10.1016/j.jmrt.2022.02.106
7. Benedetti, M., Torresani, E., Leoni, M., Fontanari, V., Bandini, M., Pederzolli, C., & Potrich, C. (2017). The effect of post-sintering treatments on the fatigue and biological behavior of Ti-6Al-4V ELI parts made by selective laser melting. Journal of the Mechanical Behavior of Biomedical Materials, 71, 295–306. https://doi.org/10.1016/j.jmbbm.2017.03.024
8. Antonysamy, A. A., Meyer, J., & Prangnell, P. B. (2013). Effect of build geometry on the β-grain structure and texture in additive manufacture of Ti6Al4V by selective electron beam melting. Materials Characterization, 84, 153–168. https://doi.org/10.1016/j.matchar.2013.07.012
9. Vayssette, B., Saintier, N., Brugger, C., Elmay, M., & Pessard, E. (2018). Surface roughness of Ti-6Al-4V parts obtained by SLM and EBM: Effect on the High Cycle Fatigue life. Procedia Engineering, 213, 89–97. https://doi.org/10.1016/j.proeng.2018.02.010
10. Madhukar, S., Sai, V. P., Kumar, S., & Prakash, D. J. (2017). Experimental investigation on effect of heat treatment on mechanical properties of steels and titanium. Int. J. Curr Eng. Technol., 7(3), 111-1112.
11. Fousová, M., Vojtěch, D., & Kubásek, J. (2016). Titanium Alloy Ti-6Al-4V Prepared by Selective Laser Melting (SLM). Manufacturing Technology, 16(4), 691–697. https://doi.org/10.21062/ujep/x.2016/a/1213-2489/mt/16/4/691
12. Vrancken, B., Thijs, L., Kruth, J.-P., & Van Humbeeck, J. (2012). Heat treatment of Ti6Al4V produced by Selective Laser Melting: Microstructure and

mechanical properties. Journal of Alloys and Compounds, 541, 177–185. https://doi.org/10.1016/j.jallcom.2012.07.022

13. Galati, M., & Iuliano, L. (2018). A literature review of powder-based electron beam melting focusing on numerical simulations. Additive Manufacturing, 19, 1–20. https://doi.org/10.1016/j.addma.2017.11.001

14. Zhang, Y., Wu, L., Guo, X., Kane, S., Deng, Y., Jung, Y.-G., Lee, J.-H., & Zhang, J. (2017). Additive Manufacturing of Metallic Materials: A Review. Journal of Materials Engineering and Performance, 27(1), 1–13. https://doi.org/10.1007/s11665-017-2747-y

15. Zenou, M., & Grainger, L. (2018). Additive manufacturing of metallic materials. In J. Zhang & Y.-G. Jung (Eds.), Additive manufacturing (pp. 53–103). Butterworth-Heinemann. https://doi.org/10.1016/B978-0-12-812155-9.00003-7

16. Williams, S. W., Martina, F., Addison, A. C., Ding, J., Pardal, G., & Colegrove, P. (2016). Wire + Arc Additive Manufacturing. Materials Science and Technology, 32(7), 641–647. https://doi.org/10.1179/1743284715y.0000000073

17. Coykendall, J., Cotteleer, M., Holdowsky, J., & Mahto, M. (2014). 3D opportunity in aerospace and defense: Additive manufacturing takes flight (A Deloitte series on additive manufacturing, 1). Westlake, TX: Deloitte University Press.

18. Addison, A., Ding, J., Martina, F., Lockett, H., & Williams, S. (2015). Titanium Europe 2015. Birmingham (UK).

19. Frazier, W. E. (2014). Metal Additive Manufacturing: A Review. Journal of Materials Engineering and Performance, 23(6), 1917–1928. https://doi.org/10.1007/s11665-014-0958-z

20. Martina, F., Colegrove, P. A., Williams, S. W., & Meyer, J. (2015). Microstructure of Interpass Rolled Wire + Arc Additive Manufacturing Ti-6Al-4V Components. Metallurgical and Materials Transactions A, 46(12), 6103–6118. https://doi.org/10.1007/s11661-015-3172-1

21. Ríos, S., Colegrove, P. A., Martina, F., & Williams, S. W. (2018). Analytical process model for wire + arc additive manufacturing. Additive Manufacturing, 21, 651–657. https://doi.org/10.1016/j.addma.2018.04.003

22. Ho, A., Zhao, H., Fellowes, J. W., Martina, F., Davis, A. E., & Prangnell, P. B. (2019). On the origin of microstructural banding in Ti-6Al4V wire-arc based high deposition rate additive manufacturing. Acta Materialia, 166, 306–323. https://doi.org/10.1016/j.actamat.2018.12.038

23. Alonso, U., Veiga, F., Suárez, A., & Artaza, T. (2020). Experimental Investigation of the Influence of Wire Arc Additive Manufacturing on the Machinability of Titanium Parts. Metals, 10(1), 24. https://doi.org/10.3390/met10010024

24. Donoghue, J., Antonysamy, A. A., Martina, F., Colegrove, P. A., Williams, S. W., & Prangnell, P. B. (2016). The effectiveness of combining rolling deformation with Wire–Arc Additive Manufacture on β-grain refinement and texture modification in Ti–6Al–4V. Materials Characterization, 114, 103–114. https://doi.org/10.1016/j.matchar.2016.02.001

25. Castellanos, S. D., Alves, J. L., & Neto, R. J. (2017). A comparative study of manufacturing processes of complex surface parts in Titanium Ti6Al4V. Ciência & Tecnologia Dos Materiais, 29(2), 73–78. https://doi.org/10.1016/j.ctmat.2017.03.002

26. Mashigo, L., Möller, H., & Gassmann, C. (2021). Comparison of the mechanical properties of Grade 5 and Grade 23 Ti6Al4V for wire-arc additive manufacturing. Journal of the Southern African Institute of Mining and Metallurgy, 121(7). https://doi.org/10.17159/2411-9717/1498/2021

27. Zhuo, Y., Yang, C., Fan, C., Lin, S., Chen, C., & Cai, X. (2020). Microstructure and mechanical properties of wire arc additive repairing Ti–5Al–2Sn–2Zr–4Mo–4Cr titanium alloy. Materials Science and Technology, 36(15), 1712–1719. https://doi.org/10.1080/02670836.2020.1822061

28. Lin, Z., Song, K., & Yu, X. (2021). A review on wire and arc additive manufacturing of titanium alloy. Journal of Manufacturing Processes, 70, 24–45. https://doi.org/10.1016/j.jmapro.2021.08.018

29. Schwab, S., Selin, R., & Voron, M. (2023). Welding materials for TIG welding, surfacing, and WAAM technology of titanium alloys. Welding in the World, 67(4), 981–986. https://doi.org/10.1007/s40194-023-01464-z

30. Cerri, E., Ghio, E., Spigarelli, S., Cabibbo, M., & Bolelli, G. (2023). Static and dynamic precipitation phenomena in laser powder bed-fused Ti6Al4V alloy. Materials Science and Engineering: A, 880, 145315. https://doi.org/10.1016/j.msea.2023.145315

31. Ren, Y., Xu, J., Wei, Y., Liu, Y., Zhu, J., & Liu, S. (2025). Effect of Interstitial Oxygen on the Microstructure and Mechanical Properties of Titanium Alloys: A Review. Crystals, 15(7), 618. https://doi.org/10.3390/cryst15070618

32. Ahmed, T., & Rack, H. J. (1998). Phase transformations during cooling in α+β titanium alloys. Materials Science and Engineering: A, 243(1-2), 206–211. https://doi.org/10.1016/s0921-5093(97)00802-2

33. Thijs, L., Verhaeghe, F., Craeghs, T., Humbeeck, J. V., & Kruth, J.-P. (2010). A study of the microstructural evolution during selective laser melting of Ti–6Al–4V. Acta Materialia, 58(9), 3303–3312. https://doi.org/10.1016/j.actamat.2010.02.004

34. Ding, D., Pan, Z., Cuiuri, D., & Li, H. (2015). Wire-feed additive manufacturing of metal components: technologies, developments and future interests. The International Journal of Advanced Manufacturing Technology, 81(1-4), 465–481. https://doi.org/10.1007/s00170-015-7077-3

35. Vrancken, B., Thijs, L., Kruth, J.-P. ., & Van Humbeeck, J. (2014). Microstructure and mechanical properties of a novel β titanium metallic composite by selective laser melting. Acta Materialia, 68, 150–158. https://doi.org/10.1016/j.actamat.2014.01.018

36. Lütjering, G., & Williams, J. C. (2007). Titanium (2nd ed.). Springer. https://doi.org/10.1007/978-3-540-73036-1

37. Leyens, C., & Peters, M. (2003). Titanium and titanium alloys. Wiley-VCH. https://doi.org/10.1002/3527602119

38. Boyer, R., Welsch, G., & Collings, E. W. (1994). Materials properties handbook: Titanium alloys. ASM International.